Title	Resolving the Pinning Force of Nanobubbles with Optical Microscopy
Author(s)	Tan, Beng Hau; An, Hongjie; Ohl, Claus-Dieter
Citation	Tan, B. H., An, H., & Ohl, C.-D. (2017). Resolving the Pinning Force of Nanobubbles with Optical Microscopy. Physical Review Letters, 118(5), 054501-.
Date	2017
URL	http://hdl.handle.net/10220/42573
Rights	© 2017 American Physical Society (APS). This paper was published in Physical Review Letters and is made available as an electronic reprint (preprint) with permission of American Physical Society (APS). The published version is available at: [https://doi.org/10.1103/PhysRevLett.118.054501]. One print or electronic copy may be made for personal use only. Systematic or multiple reproduction, distribution to multiple locations via electronic or other means, duplication of any material in this paper for a fee or for commercial purposes, or modification of the content of the paper is prohibited and is subject to penalties under law.

Resolving the Pinning Force of Nanobubbles with Optical Microscopy

Beng Hau Tan (陈明豪), Hongjie An (安红杰),* and Claus-Dieter Ohl†
Cavitation Lab, Division of Physics and Applied Physics, School of Physical and Mathematical Sciences, Nanyang Technological University, Singapore 637371, Singapore
(Received 8 September 2016; revised manuscript received 16 December 2016; published 31 January 2017)

Many of the remarkable properties of surface nanobubbles, such as unusually small contact angles and long lifetimes, are related to the force that pins them onto their substrates. This pinning force is yet to be quantified experimentally. Here, surface-attached nanobubbles are pulled with an atomic force microscope tip while their mechanical responses are observed with total internal reflection fluorescence microscopy. We estimate that a pinning force on the order of 0.1μN is required to unpin a nanobubble from its substrate. The maximum force that the tip can exert on the nanobubble is limited by the stability of the neck pulled from the bubble and is enhanced by the hydrophobicity of the tip.

DOI: 10.1103/PhysRevLett.118.054501

Surface nanobubbles are gaseous domains attached onto wetted surfaces. They possess unusual properties, such as long lifetimes and anomalously small contact angles, both of which remain to be fully understood [1–3]. The key to both properties is thought to be the experimentally observed contact line pinning of nanobubbles, which constrains them to grow or shrink only in height, while their footprints remain fixed. Although no single explanation for the long lifetimes of nanobubbles has gained wide acceptance, a strong consensus has emerged from theoretical, experimental, and computational studies [4–9] that substrate pinning is essential for nanobubble stability. Moreover, a popular explanation for the unusually small contact angles of nanobubbles observed in experiments is that line pinning manifests as a line tension τ, changing the bubble's nanoscopic contact angle predicted by Young's law, $\cos\theta_c = (\gamma_{sv} - \gamma_{sl})/\gamma$, to $\cos\theta = \cos\theta_c - \tau/\gamma R$, where R is the radius of curvature and the subscripts in γ refer to the solid, liquid, and vapor phases.

Although it is now agreed that nanobubbles are strongly pinned to their surfaces, the pinning strength has never been determined accurately. Experimental efforts to quantify contact line pinning have centered on a direct measure of the pinning force or line tension. Traditionally, most research groups favor the line tension approach, since this quantity can be easily computed by fitting a distribution of nanobubble contact angles and radii to three-dimensional atomic force microscopy (AFM) data [1]. Unfortunately, this method leads to conflicting estimates for τ [10–14] that span 3 orders of magnitude, in both positive and negative values [1]. An alternative approach is to subject nanobubbles to strong forces, in the hopes of triggering their unpinning or destruction. Remarkably, however, no method has yet been known to unpin nanobubbles, even when they are subjected to intense contact mode scanning in AFM [15] or cavitation-induced shock waves [16]. The magnitude of the substrate pinning therefore remains an open question.

An understanding of pinning is also important in controlling the distribution of surface-attached bubbles for applications such as the reduction of drag in microfluidics [17,18], surface cleaning [19], and even graphene transfer [20]. In typical nucleation experiments, exchanging water and organic solvent over a surface [21] creates an uncontrollable distribution of bubbles on the substrate. To tailor the use of nanobubbles for specific applications, it is also important to understand how large a force is required to move or destroy these objects if they appear in undesirable locations.

Even though it has long been desired to measure the strength of the contact line pinning, widely used methods such as AFM cannot provide the dynamic imaging required to understand how strong forces interact with nanobubbles, or to observe the threshold at which nanobubbles can unpin from their substrate. In this Letter, we extend the current understanding of contact line pinning by utilizing the precise manipulation ability of AFM to pull bubbles with a tip, while visualizing their mechanical responses optically with total internal reflection fluorescence microscopy (TIRFM). We show that this method is capable of unpinning a nanobubble from its substrate and derive an estimate of the pinning force.

Micro- and nanobubbles are nucleated on a glass cover slip (no. 1, Menzel-Gläser, Germany) by exchanging water, ethanol, and water within the confines of a polydimethylsiloxane (PDMS) microchannel [Fig. 1(a)]. 2.5 μM of rhodamine 6G (Sigma-Aldrich, Germany) fluorescent dye was added to both exchange liquids to visualize the bubbles in TIRFM. PDMS channels were fabricated with standard techniques and plasma cleaned for 30 s before bonding them onto the cover slip in a low-humidity, room temperature environment for 24 h. This ensures that the channel is removable for AFM characterization, while providing sufficient sealing to avoid leakage of liquids during nanobubble nucleation. Although contamination from PDMS is known

to be a significant issue in nucleation experiments—leading to the formation of oil droplets instead of nanobubbles—we have verified that objects nucleated using the above-mentioned protocol are gaseous [22].

In TIRFM, a laser beam ($\lambda = 532$ nm) is steered through a 60× oil-immersion microscope objective (Olympus, Japan) and reflects internally on the bottom of a glass cover slip, generating a evanescent region above its top surface [23]. Under excitation by the evanescence, dye attached onto the bubbles fluoresces, and when the excitation is removed using suitable filters, nanobubbles appear as highly contrasted regions against the dark background, as shown in Fig. 1(b). To ensure that the nanobubbles remain immersed during AFM characterization, a reservoir of 1 ml of deionized water is dispensed around the channel before removing it. The nanobubbles are then imaged in tapping mode AFM (Bioscope Catalyst, Bruker, U.S.) using a gold-coated cantilever (NSC-19/Cr-Au, MikroMasch) with a nominal spring constant $k = 0.5$ N/m. The AFM tips are hydrophobic when used as received, but plasma cleaning (Harrick Plasma, United States) for 20 s renders them hydrophilic.

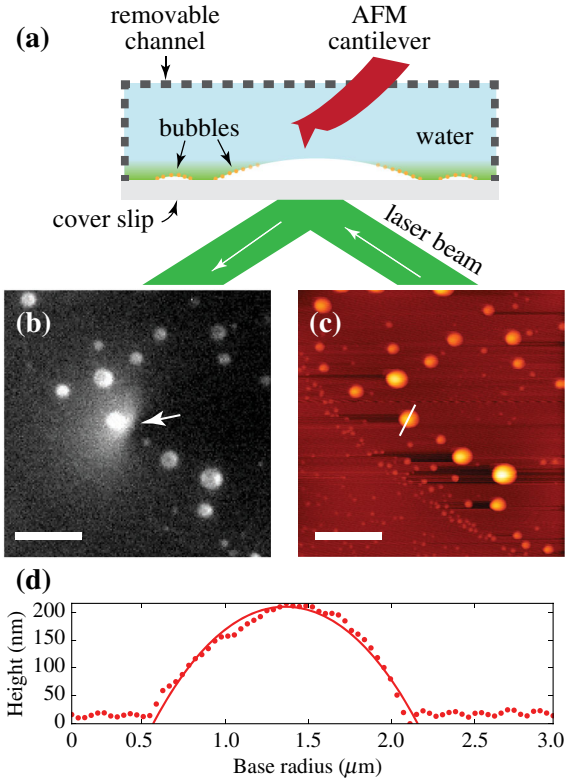

FIG. 1. Simultaneous microscopy of nanobubbles. (a) Bubbles are nucleated by solvent exchange within a removable channel. (b) TIRFM image of the bubbles. (c) AFM image of the same feature. A bright spot in the middle (white arrow) corresponds to the location of the AFM tip. The scale bars in (b) and (c) are 5 μm. (d) AFM-measured height profile of a bubble marked in white in (c), fitted to a spherical cap (red line). The fitted contact angle is 28.2°.

Simultaneous AFM-TIRFM images [Figs. 1(b) and 1(c)] of a 20×20 μm^2 area show the advantages of each imaging mode. Optical microscopy allows dynamic imaging over areas of $\sim 100 \times 100$ μm^2. On the other hand, the superior spatial resolution of AFM is evident, embodied by the appearance of tiny nanobubbles that are not visible in the optical image due to the diffraction limit [Fig. 1(c)]. An AFM height profile of one of the bubbles is shown in Fig. 1(d) and is fitted to a spherical cap by the least-squares method (red line). The fitted contact angle of 28.2° is defined from the less dense gas phase and is consistent with previous reports [1–3]. However, this angle should not be considered definitive, since the contribution of dye to the interfacial energy balance at the bubble's three-phase line may alter the contact angle from a "pure" system.

The precise control provided by AFM allows the mechanical response of nanobubbles to pulling to be measured. A schematic of the experiment is depicted in Fig. 2(a). In tapping mode AFM, the tip's oscillation amplitude is kept constant by a feedback mechanism that monitors the input amplitude signal with respect to a setpoint. A lower setpoint corresponds to a larger amplitude drop and a stronger tip-sample interaction.

Careful control of the lateral position of the tip as well as the tip-object contact allows individual nanobubbles to be manipulated. First, the tip is maneuvered to a position just inside the footprint of a selected nanobubble without contacting it (here, a setpoint beyond 100% is used). Second, the tip is made to anchor onto the bubble and contact the substrate strongly by reducing the setpoint to 10%. Third, the bubble is pulled laterally over the substrate by adjusting its position via software control. Note that in our AFM setup, the stage containing the substrate and bubbles is moved, while the lateral position of the AFM tip is fixed at all times. Optical imaging in TIRFM is captured at 10 frames/s.

Moving a tip that is anchored to a nanobubble causes a neck to extend from it, as we show for hydrophobic and hydrophilic tips in Figs. 2(b) and 2(c). In most cases, the neck can only be pulled out for a limited distance before it becomes unstable and pinches off, as shown in Fig. 2(b) for a hydrophilic tip. In some cases, the necks pulled by a hydrophobic tip resist collapse, which allows them to be extended with sufficient force to unpin from their substrate; see $t = 50$–60 s in Fig. 2(c). No bubbles were successfully unpinned with a hydrophilic tip.

The ability to observe the deformation of bubbles by the AFM tip allows the pulling force induced by the tip to be estimated. The work done by the tip pulling out a neck of length h from the bubble leads to a change in surface energy $\gamma \Delta S$ in the bubble, where γ is the surface tension and $\Delta S = S_{\text{pulled}} - S_{\text{unpulled}}$ is the difference in surface energy between the unpulled, spherically capped nanobubble, and at its maximal extension. Equating these terms leads to

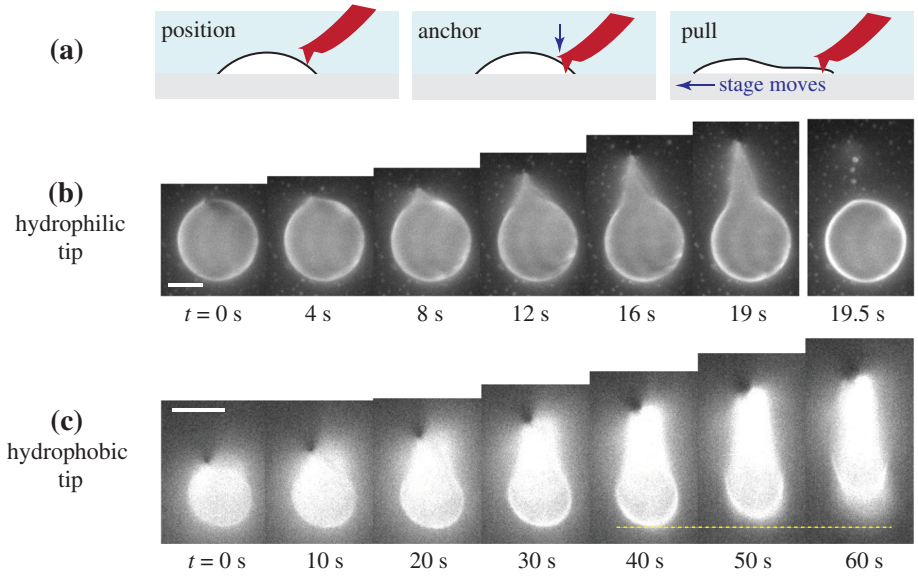

FIG. 2. Pulling of nanobubbles. (a) A schematic of the bubble pulling experiment. Note that in our setup the AFM tip is always at a fixed lateral position, while the stage and the bubbles are moved by software control. (b) TIRFM image of a microbubble as it is pulled by a hydrophilic tip. (c) TIRFM image of a bubble pulled by a hydrophobic tip. Over the last 20 s the bubble unpins and slides across the substrate. The scale bars in (b) and (c) are 5 μm.

$$F = \frac{\gamma \Delta S}{h}. \tag{1}$$

We estimate ΔS from the optical TIRFM images by detecting the footprint, calculating the effective radius of curvature, and taking a surface of revolution about the bubble's axis of symmetry while enforcing the experimentally observed contact angle of the nanobubble in the integration. More details are presented in the Supplemental Material [24].

The calculated values of the maximum force F exerted by the tip are shown in Fig. 3(a). The nanobubbles that survived the pulling were subjected to $F \sim 0.05$ μN before their necks collapsed, while those that were successfully unpinned were generally subjected to $F \sim 0.1$ μN. Since the neck length h is the maximum extension just before the nanobubble starts to slide along the substrate, the maximum force exerted by the tip on the unpinned bubbles is equivalent to the pinning force by the substrate for the bubbles, denoted by green points in Fig. 3(a). As the absolute pinning force varies with the nanobubble's size, we also plot the pinning strength, the force normalized by the footprint perimeter of the unpulled nanobubble $F/2\pi L$ in Fig. 3(b). The normalization identifies a threshold pinning strength of about 5 mN/m, which reaches up to ~20 mN/m. Variations in pinning strength are presumably due to chemical and physical heterogeneities along the substrate.

This estimate of the pinning force is consistent with previous theoretical and experimental work in the literature, in particular, with the lattice density functional theory calculations of Liu *et al.* [8], which predict a pinning force per unit length within an order of magnitude of the surface tension. Our measurements also reinforce experiments that show nanobubbles comfortably surviving up to 50 nN of force from invasive contact mode AFM scanning [25].

It is clear from our experiments that the maximum force exerted by the tip on the bubble depends on the stability of the neck that is pulled out by the tip, since the neck collapses beyond a certain extension. The neck is a

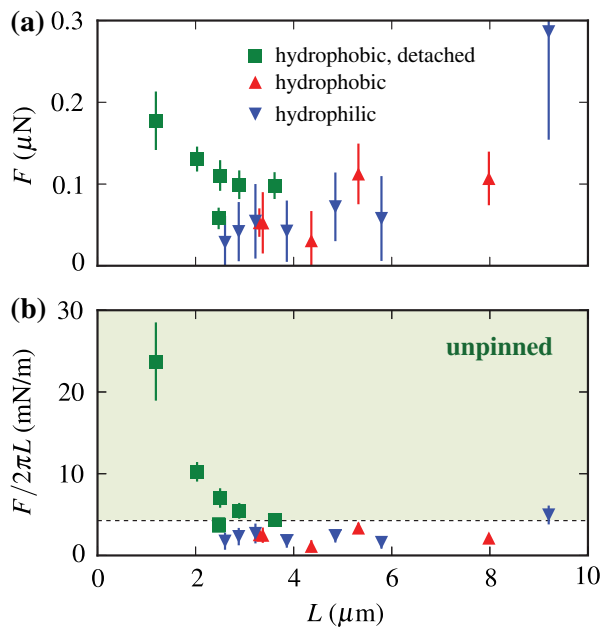

FIG. 3. (a) Pulling force F [calculated from Eq. (1)] on nanobubbles and (b) F normalized by the perimeter of the unpulled bubble.

minimum energy surface [26–28] formed by an interface which spans two coaxial rings separated by a distance x. Since the free energy of the interface is proportional to its surface area, the minimal energy configuration of the interface is equivalent to finding its minimal surface area. This surface of revolution is $S[r] = 2\pi \int r\sqrt{1+(\dot{r})^2}dr$. The interfacial profile $r(x)$ that generates the minimal surface area can then be found from variational calculus to be $r\ddot{r} = 1 + \dot{r}^2$. The general solution of this equation is the catenary [29]

$$r(x) = a\cosh(x/a + c), \tag{2}$$

where a and c are constants determined by the boundary conditions.

This argument can be extended to the neck pulled out of a surface-attached nanobubble, a schematic of which is shown in Fig. 4. The neck, whose cross section is a truncated sphere, can also be described by a catenary since the angular dependence factor 2π drops out during the derivation of Eq. (2) [30]. The boundary conditions at the two footprint radii at each end of the neck are then

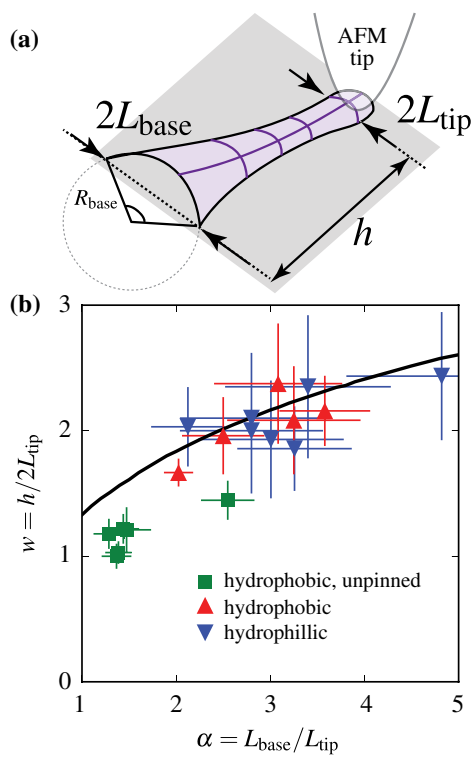

FIG. 4. Stability of the neck pulled from a bubble. (a) The neck region describes a catenoid with footprint radius L_{base} at the bubble's base, L_{tip} at the tip, and length x (see Fig. 2 for a top view). (b) The stability threshold of the neck as a function of $w = h/2L_{tip}$ and $\alpha = L_{base}/L_{tip}$. Points that lie above the theoretical curve (black line) are unstable. The experimental points (green squares) represent bubbles unpinned from their substrates by hydrophobic tips; these points notably fall within the stable region.

$L_{tip} = a\cosh c$ and $L_{base} = a\cosh(h/a + c)$. The classical calculation requires the radius of curvature R [see Fig. 4(a)], but this cannot be resolved in our experiment. Instead, we utilize the experimentally observable footprint radii L. We justify this by noting that a spherical cap with constant contact angle θ obeys $L = R\sin\theta$ and, thus, $L_{base}/L_{tip} = R_{base}/R_{tip}$. By also defining $X = L_{tip}/a$, $w = h/2L_{tip}$, and $\alpha = L_{base}/L_{tip}$, Salkin *et al.* [31] showed that the equation for L_{base} can be expressed as the nonlinear equation

$$\sinh^2(wX) - X^2[1 - 2\alpha\cosh(wX) + \alpha^2] = 0. \tag{3}$$

A stable neck exists when one or more roots for Eq. (3) can be found. By iteratively searching for roots with a parameter sweep of X and w, it can be shown that every unique neck configuration $\alpha = L_{base}/L_{tip}$ possesses a unique maximum stretching length h (see the Supplemental Material [24]). After the neck is stretched beyond its threshold length h_{max}, Eq. (3) has no roots and the neck is no longer stable. (Note that the boundary values a and c do not influence h_{max}.) This calculation is then repeated for $1 < \alpha < 5$ to obtain the stability threshold curve in Fig. 4(b). Our experiments show reasonable agreement with the stability theory [Fig. 4(b)]—the bubbles tolerate a certain amount of stretching before the neck becomes unstable and pinches off. We also find that the bubbles which successfully unpin and start to slide along the substrate [green square points, Fig. 4(b)] lie within the stable region, as expected.

The preceding analysis suggests that the key to unpinning nanobubbles from their substrate lies in a relatively large neck radius L_{tip} and low α, which promotes neck stability. It is also apparent from Figs. 2(b) and 2(c) that hydrophobic tips are more likely to unpin nanobubbles, since the necks that they pull out from the nanobubbles are considerably wider than the thin ones pulled out by hydrophilic tips. However, it is not immediately clear why hydrophobic tips have significant variation in the neck width, leading to some nanobubbles unpinning and others not. It is likely that the hydrophobic tips in our experiments, which are not cleaned, contain some nano-rough heterogeneities leading to a spread in observed contact angles at the neck.

In conclusion, we have measured the pinning force on nanobubbles by stretching them with a precisely maneuvered AFM tip to the point that they begin to slide along the substrate. For a nanobubble to be successfully unpinned, the neck pulled out by the tip must be stable against pinch-off, a condition that is facilitated by the tip wettability. Our results have implications not only in understanding fundamental properties of nanobubbles that are still elusive, but also in controllably decorating surfaces with nanobubbles for various industrial applications.

We thank David Quéré for discussions. We acknowledge funding from a competitive research program under the

auspices of the Singapore government's National Research Foundation (Program No. NRF-CRP9-2011-04). B. H. T. acknowledges financial support from the Agency of Science, Technology and Research in Singapore.

*Corresponding author.
hjan@ntu.edu.sg
†cdohl@ntu.edu.sg

[1] J. R. T. Seddon and D. Lohse, J. Phys. Condens. Matter **23**, 133001 (2011).
[2] D. Lohse and X. Zhang, Rev. Mod. Phys. **87**, 981 (2015).
[3] V. S. J. Craig, Soft Matter **7**, 40 (2011).
[4] X. Zhang, D. Y. C. Chan, D. Wang, and N. Maeda, Langmuir **29**, 1017 (2013).
[5] J. H. Weijs and D. Lohse, Phys. Rev. Lett. **110**, 054501 (2013).
[6] Y. Liu and X. Zhang, J. Chem. Phys. **138**, 014706 (2013).
[7] Y. Liu and X. Zhang, J. Chem. Phys. **141**, 134702 (2014).
[8] Y. Liu, J. Wang, X. Zhang, and W. Wang, J. Chem. Phys. **140**, 054705 (2014).
[9] D. Lohse and X. Zhang, Phys. Rev. E **91**, 031003 (2015).
[10] J. Yang, J. Duan, D. Fornasiero, and J. Ralston, J. Phys. Chem. B **107**, 6139 (2003).
[11] N. Kameda and S. Nakabayashi, Chem. Phys. Lett. **461**, 122 (2008).
[12] M. A. J. van Limbeek and J. R. T. Seddon, Langmuir **27**, 8694 (2011).
[13] W. Guo, H. Shan, M. Guan, L. Gao, M. Liu, and Y. Dong, Surf. Sci. **606**, 1462 (2012).
[14] K. K. Rangharajan, K. J. Kwak, A. T. Conlisk, Y. Wu, and S. Prakash, Soft Matter **11**, 5214 (2015).
[15] M. Holmberg, A. Kühle, K. A. Mørch, and A. Boisen, Langmuir **19**, 10510 (2003).
[16] B. M. Borkent, S. M. Dammer, H. Schönherr, G. J. Vancso, and D. Lohse, Phys. Rev. Lett. **98**, 204502 (2007).
[17] E. Lauga and H. A. Stone, J. Fluid Mech. **489**, 55 (2003).
[18] E. Karatay, A. S. Haase, C. W. Visser, C. Sun, D. Lohse, P. A. Tsai, and R. G. H. Lammertink, Proc. Natl. Acad. Sci. U.S.A. **110**, 8422 (2013).
[19] G. Liu and V. S. J. Craig, ACS Appl. Mater. Interfaces **1**, 481 (2009).
[20] L. Gao, G.-X. Ni, Y. Liu, B. Liu, A. H. Castro Neto, and K. P. Loh, Nature (London) **505**, 190 (2014).
[21] S.-T. Lou, Z.-Q. Ouyang, Y. Zhang, X.-J. Li, J. Hu, M.-Q. Li, and F.-J. Yang, J. Vac. Sci. Technol. B **18**, 2573 (2000).
[22] C. U. Chan, L. Chen, M. Arora, and C.-D. Ohl, Phys. Rev. Lett. **114**, 114505 (2015).
[23] C. U. Chan and C.-D. Ohl, Phys. Rev. Lett. **109**, 174501 (2012).
[24] See Supplemental Material at http://link.aps.org/supplemental/10.1103/PhysRevLett.118.054501 for details on the preparation of the glass substrate, calculation of the bubbles' surface energies from experimental footprints and derivation of the stability threshold.
[25] H. An, B. H. Tan, and C.-D. Ohl, Langmuir **32**, 12710 (2016).
[26] D. H. Michael, Ann. Rev. Fluid Mech. **13**, 189 (1981).
[27] M. Reyssat and D. Quéré, J. Phys. Chem. B **113**, 3906 (2009).
[28] H. M. Princen, J. Colloid. Interf. Sci. **34**, 171 (1970).
[29] K. F. Riley, M. P. Hobson, and S. J. Bence, *Mathematical Methods for Physics and Engineering: A Comprehensive Guide* (Cambridge University Press, Cambridge, England, 2006), pp. 736–737.
[30] The angular independence also explains why a one-dimensional hanging chain satisfies the same cosh x dependence as a soap film between coaxial rings.
[31] L. Salkin, A. Schmit, P. Panizza, and L. Courbin, Am. J. Phys. **82**, 839 (2014).